APL Materials

Silicon nanowire arrays coated with electroless Ag for increased surface-enhanced Raman scattering

Cite as: APL Mater. **3**, 056101 (2015); https://doi.org/10.1063/1.4921040
Submitted: 07 March 2015 • Accepted: 30 April 2015 • Published Online: 11 May 2015

Fan Bai, Meicheng Li, Pengfei Fu, et al.

Silicon nanowire arrays coated with electroless Ag for increased surface-enhanced Raman scattering

Fan Bai,[1,2] Meicheng Li,[1,3,a] Pengfei Fu,[1] Ruike Li,[1] Tiansheng Gu,[1] Rui Huang,[1] Zhao Chen,[1] Bing Jiang,[1] and Yingfeng Li[1]
[1]*State Key Laboratory of Alternate Electrical Power System with Renewable Energy Sources, North China Electric Power University, Beijing 102206, China*
[2]*National Quality Supervision and Inspection Center for Non-ferrous Metals Produces, Yunnan Institute of Products Quality Supervision and Inspection, Kunming 650223, China*
[3]*Chongqing Materials Research Institute, Chongqing 400707, China*

(Received 7 March 2015; accepted 30 April 2015; published online 11 May 2015)

The ordered Ag nanorod (AgNR) arrays are fabricated through a simple electroless deposition technique using the isolated Si nanowire (SiNW) arrays as the Ag-grown scaffold. The AgNR arrays have the single-crystallized structure and the plasmonic crystal feature. It is found that the formation of the AgNR arrays is strongly dependent on the filling ratio of SiNWs. A mechanism is proposed based on the selective nucleation and the synergistic growth of Ag nanoparticles on the top of the SiNWs. Moreover, the special AgNR arrays grown on the substrate of SiNWs exhibit a detection sensitivity of 10^{-15}M for rhodamine 6G molecules, which have the potential application to the highly sensitive surface-enhanced Raman scattering sensors. [http://dx.doi.org/10.1063/1.4921040]

Ag nanostructures can strongly increase surface-enhanced Raman scattering (SERS) signals of organic molecules and have been successfully exploited as SERS sensors to rapidly and accurately detect organic molecules.[1–3] The morphologies of Ag nanostructures and their geometric parameters strongly affect the detection sensitivity for the Ag-based increased SERS substrates. For examples, Ag nanoparticles (AgNPs) with appropriate size and narrow gaps can excite the hot spots effect and can be used as the SERS substrate to detect the low concentration (10^{-7} mol/l) of malachite green.[4] Ag nanowire monolayer also serves as an excellent SERS substrate showing a low detection limit of 10^{-10} mol/l for rhodamine 6G (R6G).[1] Furthermore, arrays of the Ag nanorod (AgNR) provide large surface areas for attaching numerous organic molecules, which is beneficial to further improve the detection sensitivity of organic molecules.[5,6] Therefore, simple preparation of the AgNR arrays is of great significance for the development of highly sensitive SERS sensors.

A few methods, including the vacuum-based sputtering[7–10] and the electrochemical deposition,[11–13] have been developed to fabricate the AgNR arrays. However, these methods require either the complicated procedures or the expensive templates, which increase the complexity and the cost. Recently, a simple and low-cost electroless deposition technique is utilized to grow the Ag nanostructures on the three-dimensional semiconductor scaffolds such as Si nanowire (SiNW) arrays,[14–18] ZnO nanorod arrays,[6] and TiO_2 nanorod arrays.[19] In the electroless deposition process, it is well known that the structural characteristic of the scaffolds affects the morphology of the Ag nanostructures. For example, the bundle-like SiNW scaffold conventionally induces the formation of Ag nanoparticles[14,15] or Ag dendrites.[20] However, the AgNR arrays based on SiNWs have not been achieved in the previous reports so far.

To produce the AgNR arrays, we consider that the isolated SiNWs could be used as the Ag-grown substrate. The isolated SiNW scaffold has the following advantages: first, the Ag-nucleation

[a]Author to whom correspondence should be addressed. Electronic mail: mcli@ncepu.edu.cn. Fax: 86-10-6177-2951.

sites are located at the tip of the single SiNWs; second, the growth orientation of the Ag nanorod is limited along the axial direction of the single SiNWs.

In this work, the arrays of the isolated SiNWs are selected as the scaffolds to grow Ag nanostructure by the electroless deposition process. The ordered AgNR arrays with the single-crystallize and plasmonic crystal features are achieved. The influence of the filling ratios of SiNW arrays on the formation of the AgNR arrays has been investigated, and the corresponding growth mechanism is proposed. Furthermore, it has been demonstrated that the ordered AgNR arrays are capable to perform the highly sensitive detection of R6G molecules.

The isolated SiNW arrays are fabricated using the previously reported process.[21] The SiNW arrays are immersed into 5% HF solution for 3 min to produce Si–H bonds surface. And, the cleaned SiNW arrays are immediately immersed into a silver-plating solution containing 4.2M HF and 0.02M $AgNO_3$ for a short duration at room temperature. After the plating, the samples are repeatedly rinsed with deionized water and then dried in nitrogen gas.

Morphologies of the samples are characterized by a scanning electron microscope (SEM) with FEI Quanta 200F and a high resolution Transmission Electron Microscope (HRTEM) with Tecnai G^2 F20. XRD patterns of the samples are obtained using a Bruker D8 Focus X-ray powder diffractometer with Cu Kα radiation. Reflection spectra of the samples are measured by a solar cell Incident Photon to Converted Electron Ratio/Quantum Efficiency (IPCE/QE) measurement system with an integrating sphere. SERS spectra of the samples are collected by a laser confocal micro-Raman spectroscopy with a LabRAM Aramis under 532 nm radiation.

Fig. 1(a) shows the SEM morphology of the AgNR arrays obtained by immersing the SiNW arrays into the silver-plating solution for 45 s. It can be seen that the ordered AgNR arrays uniformly cover on the top of the SiNW arrays. The individual nanorod (Fig. 1(b)) has 400 nm in length and 100 nm in diameter, which is nearly equal to that of the SiNWs (diameter is about 80-120 nm). From its magnified HRTEM image (Fig. 1(c)), it can be seen that the nanorod is single crystalline and contains some lattice defects such as twin boundaries and stacking faults, which are further verified by the typically twinned diffraction spots in the inset image of Fig. 1(c). A selective-area Energy-dispersive X-ray Spectroscopy (EDX) analysis indicates that the nanorod is only composed of the silver element (Fig. 1(d)).

Fig. 1(e) displays an XRD pattern of the AgNR arrays, whose diffraction peaks are corresponding to (111), (200), and (220) reflections of the face-centered cubic structure of bulk silver,

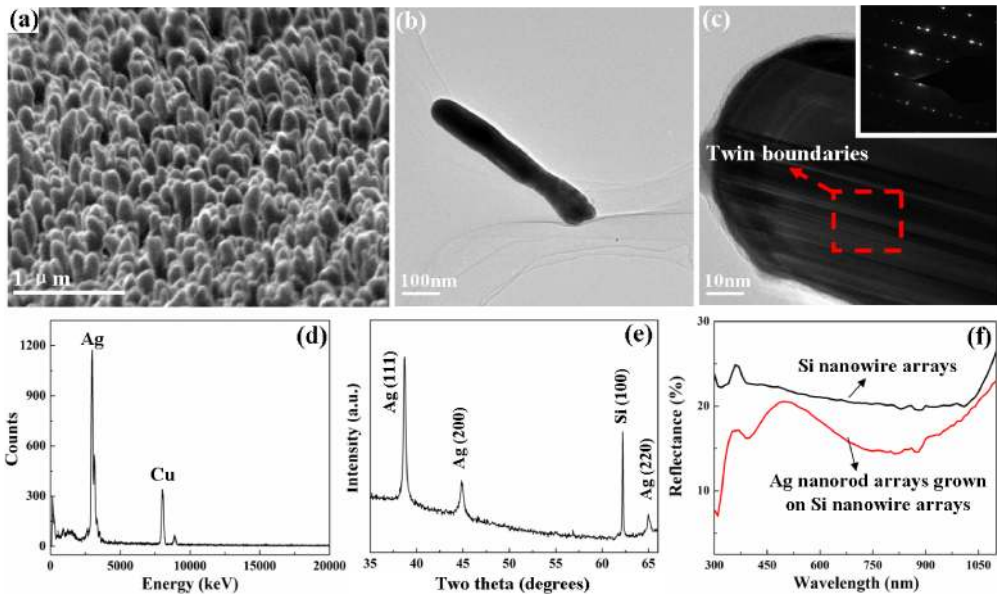

FIG. 1. Tilted SEM images of the ordered AgNR arrays (a), TEM image (b), HRTEM image (c), and EDX spectrum (d) of the individual nanorod; inset in (c) shows a selective-area electron diffraction pattern of the nanorod; (e) XRD pattern of the ordered AgNR arrays; (f) comparison of reflection spectra between the pristine SiNW arrays and the ordered AgNR arrays.

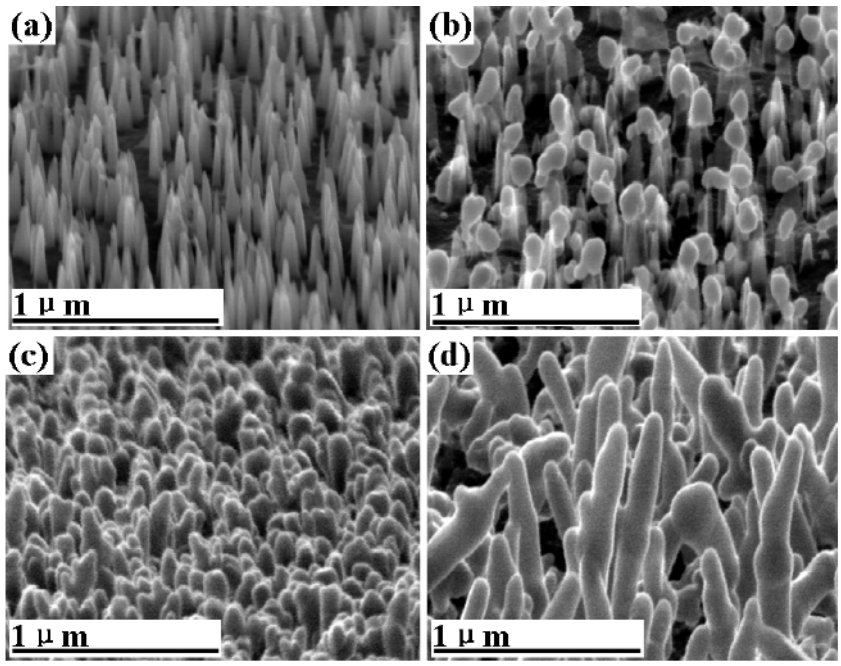

FIG. 2. Tilted SEM images of the ordered AgNR arrays on the SiNW arrays for different growing durations. (a) 0 s, (b) 10 s, (c) 30 s, (d) 60 s.

suggesting that the AgNR arrays are a well-crystallized structure. Moreover, the diffraction peak at 62° possibly originates from the diffraction of crystalline Si(100) substrate underneath the AgNR arrays. The reflection spectra of the SiNW arrays and the AgNR arrays are shown in Fig. 1(f). Compared to the pristine SiNW arrays, the AgNR arrays can suppress reflection sharply at the wavelength of 390 nm and broadly around the wavelength of 810 nm because of their plasmonic resonances effect,[3] implying its structural feature of plasmatic crystal.

To understand the growing process of the AgNRs on the SiNWs in the silver-plating solution, the morphologies of these Ag nanostructures during different growth durations are characterized. The morphology of the *in situ* SiNW arrays is shown in Fig. 2(a). After immersing the SiNW arrays in HF/$AgNO_3$ solution for 10 s, majority of Ag nanoparticles are deposited on the tips of the SiNWs (Fig. 2(b)). Meanwhile, there are rarely Ag nanoparticles at the sidewalls of the SiNWs and their bottom surfaces. With the increasing of growth time, the as-deposited Ag nanoparticles gradually grow along the axial direction of the SiNWs. When the growth time is increased to 30 s, the ordered AgNR arrays are formed on the SiNW arrays (Fig. 2(c)). These results suggest that the substrate of SiNW arrays provides a template to grow the ordered AgNR arrays.

Furthermore, we find that the morphology of AgNR arrays dramatically changes depending on the reaction conditions, especially on the growth time and the concentration of $AgNO_3$. Further increase of growth duration changes the morphology of the grown silver from ordered AgNR arrays to disordered AgNR arrays (Fig. 2(d)) and further to numerous Ag dendrites. Moreover, under lower concentrated $AgNO_3$ (i.e., 0.002M), we observe Ag nanoparticles rather than AgNR arrays. Therefore, a careful control of process parameters is necessary to obtain the ordered AgNR arrays.

The effect of the surface morphology of Si samples on the formation of AgNR arrays is investigated. Here, these Si samples include flat Si, random pyramids, and one-step etched SiNW arrays, and their surface morphologies are shown in Figs. 3(a)–3(c), respectively. When they are immersed in HF/$AgNO_3$ solution for a short time, the Ag nanoparticles are observed on the any Si samples used here. However, differences between surface morphologies of these Si samples lead to the selective nucleation behavior of the Ag nanoparticles. For the sample of flat Si, the uniform Ag nanoparticles are observed on the whole surfaces of Si (Fig. 3(d)). When the Si sample with random pyramids is used, majority of Ag nanoparticles form preferentially on the edges of these

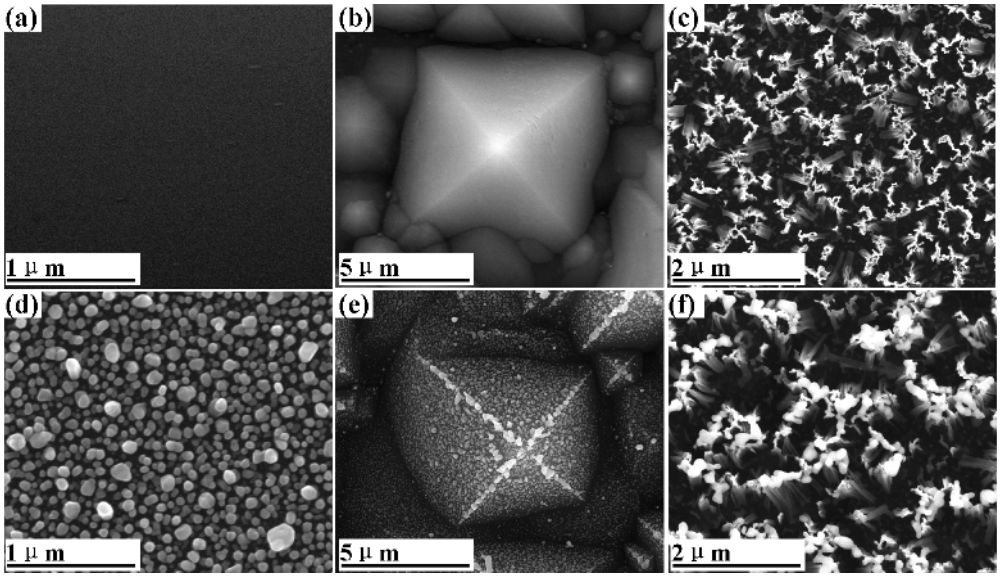

FIG. 3. Plan-view SEM images of the Si samples with different surface morphologies. (a) Flat Si, (b) random pyramid, (c) one-step etched SiNW arrays; ((d), (e), and (f)) SEM images of the Si samples with different surface morphologies after depositing Ag nanoparticles, respectively.

pyramids comparing to their sidewalls (Fig. 3(e)). In the case of one-step etched SiNW arrays, a quite large number of Ag nanoparticles are anchored on the tips of these SiNWs, as shown in Fig. 3(f). These results demonstrate that the SiNW scaffold improves the selective nucleation of the Ag nanoparticles.

Moreover, the effect of the filling ratios of SiNW arrays on the morphology of the AgNR arrays is studied. Figs. 4(a) and 4(b) show the morphologies of the SiNW arrays with different filling ratios, which can be tuned by varying the pattern between Ag catalysts.[21] The filling ratio of SiNWs is 4.9×10^7 mm^{-2} (Fig. 4(a)) and 9.3×10^7 mm^{-2} (Fig. 4(b)), respectively. Under the same deposition conditions, we find that the ordered AgNR arrays are formed on the top surface of the sparse SiNWs (Fig. 4(c)). Correspondingly, the disordered fractal AgNRs are observed on the top surface of the dense SiNWs (Fig. 4(d)). These results suggest that the filling ratio of the SiNW arrays is an important factor affecting the formation of the ordered AgNR arrays.

Based on the above results, the growth mechanism of the ordered AgNR arrays on the SiNW arrays is discussed. When the SiNW arrays (Fig. 5(a)) are immersed in a mixed solution of HF and $AgNO_3$, the nucleation of AgNPs performs preferentially on the defect areas of the SiNW arrays through the previously reported galvanic reactions.[22] Since the structural defects are more on the bare tips of SiNWs than on their other areas, the nucleation sites of AgNPs are located on the tips of SiNWs (Fig. 5(b)). Nevertheless, there are different growth modes of the AgNPs on the SiNW arrays with different filling ratios. For the sparse SiNW arrays, the AgNPs serve as the medium to transfer the electrons from the nanowire tip to the Ag^+ ions in solution, resulting in the reduction deposition of AgNPs, as described by red dashed rectangle in Fig. 5(c). However, for the dense SiNW arrays, besides the reduction growth of AgNPs, the assimilation growth among the adjacent AgNPs is also performed (Fig. 5(d)). Small AgNPs are oxidized and then assimilated into large AgNPs through the electrons transfer between NPs on the close SiNWs, which is similar to the recently reported results for the growth of AgNPs on Si wafer.[23,24] In this case, the synergistic growth of the AgNPs leads to their nonuniform distribution and disordered morphology, producing irregular Ag nanostructures such as the previously presented disordered fractal Ag nanorods (Fig. 4(d)). Therefore, the large distance between the sparse SiNWs can hinder the electron transfer between the AgNPs. Owing to a limit of the reduction reaction on the top tips of the SiNWs, the growth orientation of AgNPs is prone to be along the axial direction of the SiNWs, which is beneficial to produce the ordered Ag nanorod arrays.

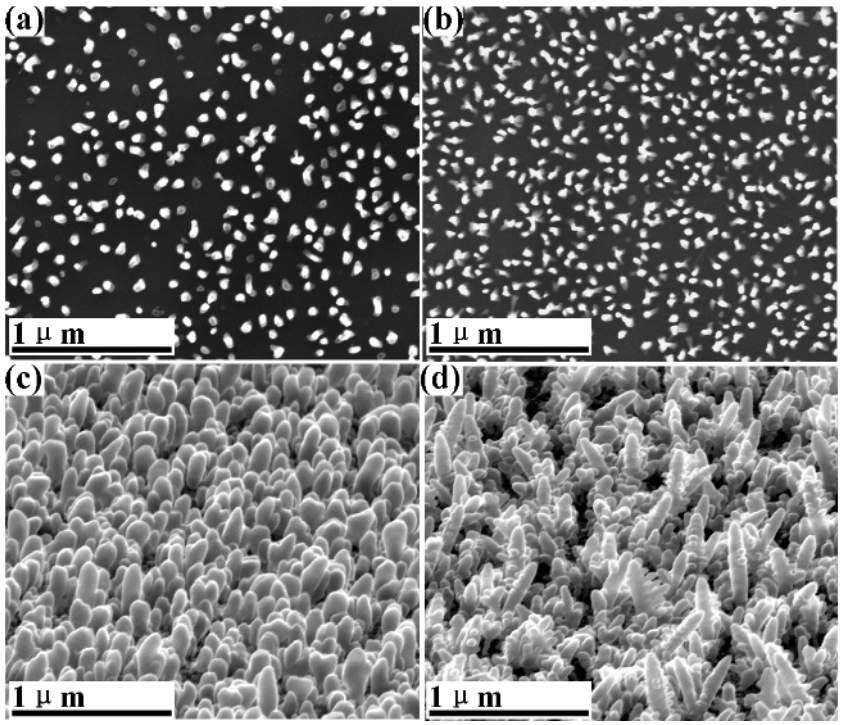

FIG. 4. Plan-view SEM images of the SiNW arrays with small (a) and large (b) filling ratios; tilted SEM images of the ordered Ag nanorod arrays (c) and the disordered fractal Ag nanorods (d) on the top of SiNW arrays corresponding to (a) and (b), respectively.

SERS property of the ordered AgNR arrays is studied using R6G as the detection molecular. Every sample is immersed in R6G solution for 10 min and then dried with nitrogen gas before testing Raman spectra. Compared to the pristine SiNW arrays, the ordered AgNR arrays can strongly increase the SERS signal intensities of R6G molecules at Raman shifts of 613, 776, 1185, 1313, 1364, 1510, 1577, and 1696 (Fig. 6(a)). To assess its SERS sensitivity, the SERS spectra of R6G at different concentrations are tested and shown in Fig. 4(b). The Raman intensity (616 cm^{-1}) monotonously reduces with lowering exponential concentrations of R6G (inset image in Fig. 6(b)). In this case, the detection concentration of R6G is as low as 10^{-15}M (Fig. 6(b)), which is lower than the values (10^{-14}M) of the detection concentration for the previously reported Ag nanoparticles-coated SiNW arrays.[17] The result indicates that the ordered AgNR arrays can be applied to the highly sensitive SERS sensors.

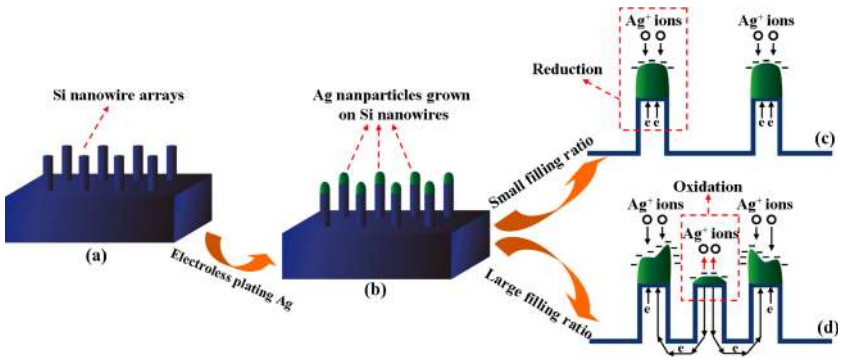

FIG. 5. Schematic diagram of the nucleation and growth of Ag nanoparticles on the SiNW arrays with different filling ratios in HF/$AgNO_3$ solution.

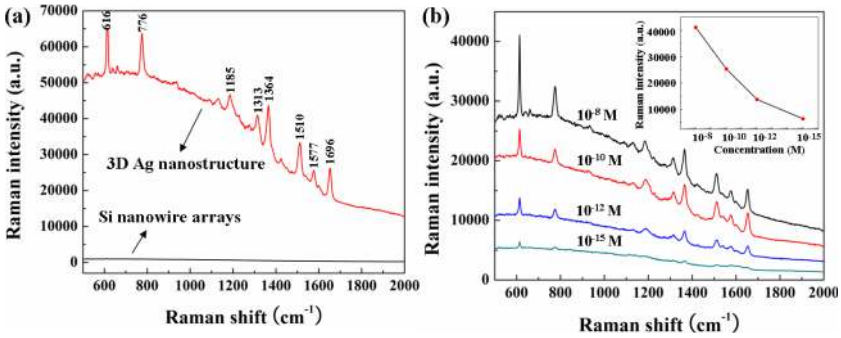

FIG. 6. (a) SERS spectra of R6G molecules at the concentration of 10^{-6}M for the SiNW arrays before and after growing ordered AgNR arrays, respectively; (b) SERS spectra of the ordered AgNR arrays at different R6G concentrations of 10^{-8}M, 10^{-10}M, 10^{-12}M, and 10^{-15}M, respectively; inset in (b) shows the relation between Raman intensity (611 cm^{-1}) and R6G concentrations.

A simple electroless deposition technique was used to grow the ordered AgNR arrays with the features of single-crystallized and the plasmonic-crystal, using the arrays of the isolated SiNWs as the substrates. It is found that the morphology of the AgNRs is affected by the filling ratio of SiNW arrays. And, the ordered AgNR arrays can only be formed on the sparse SiNW arrays. The selective nucleation and the synergistic growth of Ag nanoparticles are the key factors to form the ordered AgNR arrays. The ordered AgNR arrays exhibit a detection limit of 10^{-15}M for R6G molecules, which could be a promising candidate for highly sensitively SERS sensors.

This work is supported partially by National Natural Science Foundation of China (Grant Nos. 91333122, 51402106, 51372082, 51172069, 50972032, 61204064, and 51202067), Ph.D. Programs Foundation of Ministry of Education of China (Grant Nos. 20110036110006, 20120036120006, and 20130036110012), Par-Eu Scholars Program, and the Fundamental Research Funds for the Central Universities.

[1] A. Tao, F. Kin, C. Hess, J. Goldberger, R. R. He, Y. G. Sun, Y. N. Xia, and P. D. Yang, Nano Lett. **3**(9), 1229 (2003).
[2] C. H. Zhu, G. W. Meng, Q. Huang, Z. Zhang, Q. L. Xu, G. Q. Liu, Z. L. Huang, and Z. Q. Chu, Chem. Commun. **47**(9), 2709 (2011).
[3] J. W. Menezes, J. Ferreira, M. J. L. Santos, L. Cescato, and A. G. Brolo, Adv. Funct. Mater. **20**(22), 3918 (2010).
[4] T. Q. N. Luong, T. A. Cao, and T. C. Dao, Adv. Nat. Sci.: Nanosci. Nanotechnol. **4**(1), 015018 (2013).
[5] C. Y. Song, J. L. Abell, Y. P. He, S. H. Murph, Y. P. Cui, and Y. P. Zhao, J. Mater. Chem. **22**, 1150 (2012).
[6] G. Y. Shan, S. J. Zheng, S. P. Chen, Y. W. Chen, and Y. C. Liu, Colloids Surf., B **94**, 157 (2012).
[7] Y. Yang, Z. Y. Li, K. Yamaguchi, M. Tanemura, Z. R. Huang, D. L. Jiang, Y. H. Chen, F. Zhou, and M. Nogami, Nanoscale **4**(8), 2663 (2012).
[8] Q. Zhou, X. Zhang, Y. Huang, Z. C. Li, Y. P. Zhao, and Z. J. Zhang, Appl. Phys. Lett. **100**(11), 113101 (2012).
[9] S. Shanmukh, L. Jones, J. Driskell, Y. P. Zhao, R. Dluhy, and R. A. Tripp, Nano Lett. **6**(11), 2630 (2006).
[10] Q. Zhou, Z. C. Li, Y. Yang, and Z. J. Zhang, J. Phys. D: Appl. Phys. **41**(15), 152007 (2008).
[11] G. Sauer, G. Brehm, S. Schneider, D. Nielsch, R. B. Wehrspohn, J. Choi, H. Hofmeister, and U. Gosele, J. Appl. Phys. **91**(5), 3243 (2002).
[12] B. H. Zhang, H. S. Wang, L. H. Lu, K. L. Ai, G. Zhang, and X. L. Cheng, Adv. Funct. Mater. **18**(16), 2348 (2008).
[13] B. L. Sun, X. H. Jiang, S. X. Dai, and Z. L. Du, Mater. Lett. **63**(29), 2570 (2009).
[14] X. T. Wang, W. S. Shi, G. W. She, L. X. Mu, and S. T. Lee, Appl. Phys. Lett. **96**(5), 053104 (2010).
[15] T. Qiu, X. L. Wu, J. C. Shen, P. C. T. Ha, and P. K. Chu, Nanotechnology **17**(23), 5769 (2006).
[16] M. L. Zhang, X. Fan, H. W. Zhou, M. W. Shao, J. A. Zapien, N. B. Wong, and S. T. Lee, J. Phys. Chem. C **114**(5), 1969 (2010).
[17] E. Galopin, J. Barbillat, Y. Coffinier, S. Szunerits, G. Patriarche, and R. Boukherroub, ACS Appl. Mater. Interfaces **1**(7), 1396 (2009).
[18] X. Z. Sun, L. H. Lin, Z. C. Li, Z. J. Zhang, and J. Y. Feng, Appl. Surf. Sci. **256**(3), 916 (2009).
[19] E. Z. Tan, P. G. Yin, T. T. You, H. Wang, and L. Guo, ACS Appl. Mater. Interfaces **4**(7), 3432 (2012).
[20] K. Q. Peng and J. Zhu, Electrochim. Acta **49**, 2563 (2004).
[21] F. Bai, M. C. Li, R. Huang, Y. F. Li, M. Trevor, and K. P. Musselman, RSC Adv. **4**, 1794 (2014).
[22] F. Bai, M. C. Li, D. D. Song, H. Yu, B. Jiang, and Y. F. Li, J. Solid State Chem. **196**, 596 (2012).
[23] F. Bai, M. C. Li, R. Huang, Y. Yu, T. S. Gu, Z. Chen, H. Y. Fan, and B. Jiang, J. Nanopart. Res. **15**(9), 1915 (2013).
[24] Z. R. Smith, R. L. Smith, and S. D. Collins, Electrochim. Acta **92**, 139 (2013).